


Article

Impact of Internal Solitary Wave on Acoustic Propagation Based on Coupled Normal Mode Theory

Zhuolong Liu ¹, Yongchui Zhang ^{1,2,*} , Fei Gao ^{3,*}, Yunxiang Zhang ¹, Yang Wang ¹ and Mei Hong ^{1,2}

¹ College of Meteorology and Oceanography, National University of Defence Technology, Changsha 410003, China; lzlongnudt@nudt.edu.cn (Z.L.); zhangyunxiang@nudt.edu.cn (Y.Z.); wangyang_@nudt.edu.cn (Y.W.); hongmei17@nudt.edu.cn (M.H.)

² High Impact Weather Key Laboratory of China Meteorological Administration, Changsha 410073, China

³ Naval Research Institute, Tianjin 300061, China

* Correspondence: zyc@nudt.edu.cn (Y.Z.); gfei88_lgdx@163.com (F.G.)

Abstract: An internal solitary wave (ISW) significantly affects acoustic propagation; however, its detailed characteristics are poorly understood. Simulation experiments of sound propagation in a shallow water environment are presented to examine the effects of the source conditions and characteristics of the ISW on transmission loss (TL). The results show that the TL decreases as the depth of the source increases and the frequency of the source decreases and that the different characteristics of the ISW are highly important for estimating sound propagation when a SONAR system is in an ISW environment. Coupled normal mode theory is further employed to analyse the variations in coupling between sound field modes in an ISW environment. Further analysis reveals that the magnitude of the TL is affected by the direction and fluctuation of energy propagation between different modes, and in different ISW environments under the deep and low-frequency source conditions, the sound field energy is mainly in lower-order modes.

Keywords: internal solitary wave; sound propagation; mode coupling



Received: 18 December 2024

Revised: 9 January 2025

Accepted: 20 January 2025

Published: 21 January 2025

Citation: Liu, Z.; Zhang, Y.; Gao, F.; Zhang, Y.; Wang, Y.; Hong, M. Impact of Internal Solitary Wave on Acoustic Propagation Based on Coupled Normal Mode Theory. *J. Mar. Sci. Eng.* **2025**, *13*, 189. <https://doi.org/10.3390/jmse13020189>

Copyright: © 2025 by the authors. Licensee MDPI, Basel, Switzerland. This article is an open access article distributed under the terms and conditions of the Creative Commons Attribution (CC BY) license (<https://creativecommons.org/licenses/by/4.0/>).

1. Introduction

An internal solitary wave (ISW) is a large-amplitude wave that occurs in stratified seawater [1]. Observation studies have shown that high-amplitude nonlinear ISWs often appear on continental shelves and in shallow seas [2–4]. ISWs in shallow water environments produce significant sound velocity disturbances, which have a great influence on acoustic transmission [5–7]. Simulation studies have shown that an ISW can cause an unstable acoustic energy exchange between normal modes, which may lead to strong signal fluctuations in coastal waters [2,3,7].

The variability in the acoustic field's intensity is typically influenced by a multitude of factors, including the frequency of the source [8], depth of the source [9] and the characteristics of the ISW [10,11], such as the propagation distance, amplitude, wavelength and number, as well as the phase position between the ISW and the acoustic propagation path [10]. Headrick et al. [6,12] studied the influence of the ISW on acoustic signals, compared the simulation results with data collected by the shallow water acoustic random medium (SWARM) experiment, and reported that an ISW in the acoustic waveguide caused a significant coupling of energy between the propagating acoustic modes, resulting in broadband fluctuations in modal intensity, travel time and temporal coherence. Gao et al. [13] analysed temporal coherence under the influence of an ISW, used data from

an acoustic propagation experiment in the South China Sea and reported that the predominant oscillation periods were the same as the periods of the ISW. Katsnelson et al. [14] studied the time fluctuation of the sound field when there were wavelets in shallow water and reported that the motion of an ISW resulted in a changing acoustic interference pattern. The influence of ISWs on sound propagation further extends from a two-dimensional field to a three-dimensional field. Badiey et al. [15] observed the horizontal refraction of sound waves caused by an ISW in the SWARM experiment and verified the horizontal refraction effect of sound propagation through an ISW. Luo et al. [16] analysed the fluctuations of the low-frequency sound field in the Shallow Water 06 (SW06) experiment when an ISW appeared and observed the focusing and divergence of the sound field in the horizontal plane caused by the ISW from the received signals. Lynch et al. [17] and Lin et al. [18] studied the horizontal refraction phenomenon of sound waves in the curved channel of the ISW front and verified their conclusions with SW06 data.

With respect to the influence of ISWs on acoustic propagation [19], normal mode theory is frequently utilised to offer a detailed mechanistic interpretation of the variability in the acoustic field intensity. Dozier et al. [20,21] derived the modal amplitudes of normal modes within an internal wave environment via wave theory, established that the modal coupling coefficient was directly proportional to the horizontal gradient of the speed of sound and provided an expression for the horizontal propagation of modal amplitudes within the internal wave environment. Zhou et al. [7] reported that when the mode wavenumber difference matched the energy wavenumber of solitons, the mode coupling effect was the most obvious, resulting in an abnormal TL or large signal fluctuation. Preisig et al. [11] reported that the energy transferred between modes occurs in the range of tens of metres at the location of an ISW and was driven by the relative phase of the dominant mode. Yang et al. [22] calculated the modal coupling matrix in the presence of an ISW via the normal mode equation and applied it to the acoustic propagation model.

Although many studies have investigated the influence of ISWs on sound propagation, few scholars have considered the influence of the received sound energy when the source conditions and ISW environment change. In this work, the source conditions and characteristics of the ISW, including the number, amplitude and polarity of the ISW and position of the ISW, are fully considered, and many simulated experiments are carried out via the coupled normal mode model. The organisation of this paper is as follows. In Section 2, the data and methods are presented. The simulation results and data are analysed in Section 3. In Section 4, the results are discussed and explained via coupled normal mode theory. The main conclusions are summarised in Section 5.

2. Materials and Methods

2.1. Environmental Model Construction

An ISW is a hump-shaped unimodal wave that propagates at a stable phase velocity and maintains its shape during propagation. The ISW is the solution of some related non-linear equations [2] and can be derived from deep-sea or shallow-water ocean waveguides via various methods. The Korteweg–de Vries (KdV) equation describes the shape and propagation of solitons in shallow water, while a two-dimensional ISW can be described by the following equation [23]:

$$\eta = \eta_0 \operatorname{sech}^2 \left(\frac{(r - r_0)}{L} \right), \quad (1)$$

where η_0 is the ISW amplitude, r_0 is the centre range, and L is defined as the characteristic half-width of the soliton.

The propagation of sound waves through various superimposed waves on a three-layer layered system background is simulated. The calculation in this paper ignores the

weak functional dependence of the sound velocity on pressure and assumes that the temperature and salinity of the upper and lower layers are constant. The sound speed field $c(r, z)$ can be calculated via the following equation [24]:

$$c(r, z) = \begin{cases} c_u, & 0 < z < z_u + \eta \\ c_u + C_g(z - (z_u + \eta)), & z_u + \eta < z < z_l + \eta \\ c_l, & z_l + \eta < z < z_B \end{cases} \quad (2)$$

where r and z are the distance and the depth ($z = 0$ corresponds to the surface location), and where c_u and c_l are the sound velocities in the upper layer and lower layer, respectively. z_u is the depth of the upper layer, z_l is the depth at the boundary between the middle layer and the lower layer, and z_B is the depth of the bottom of the water. The sound speed gradient C_g in the middle layer is

$$C_g = \frac{c_l - c_u}{z_l - z_u} \quad (3)$$

Figure 1 shows the sound velocity distribution at a depth of 60 m under the influence of the ISW. The thickness of the upper mixed layer (lower mixed layer) is 15 m (30 m), and the sound speed is $c_u = 1520$ m/s ($c_l = 1494$ m/s). The sound velocity at the bottom is assumed to be $c_b = 1700$ m/s, the density at the bottom is $\rho_b = 2.0$ g/cm³ and the attenuation at the bottom is 0.6 dB per wavelength. A small-amplitude depression soliton (SADS), large-amplitude depression soliton (LADS) and large-amplitude elevation soliton (LAES) are shown in Figure 1a, and their positions are $R_i = 2$ km, $R_i = 4$ km and $R_i = 6$ km, respectively. The LADS has one ISW with $\eta_0 = 15$ m and $L = 100$ m, and the amplitudes of the SADS and LAES are $\frac{1}{4}\eta_0$ and $\frac{3}{4}\eta_0$, respectively. The large-amplitude depression packet (LADP) consists of three continuous solitons with a characteristic half-width of 100 m and amplitudes of 15 m, 12 m and 10 m, and the position of the left-hand soliton of the LADP is $R_i = 5$ km. Additionally, the amplitude of each soliton in the small-amplitude depression packet (SADP) is 1/4 that of each soliton in the LADP, and the position of the left-hand soliton in the SADP is $R_i = 1.5$ km.

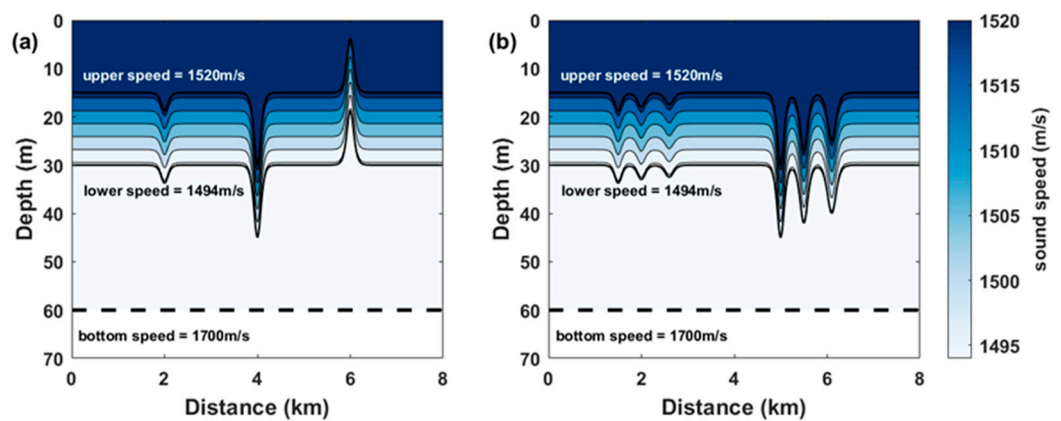


Figure 1. Schematic diagram of the sound velocity distribution under the influence of an ISW; the thermocline displacement geometries are plotted as solid black lines, and the boundaries of the bottom are plotted as dotted black lines: (a) Soliton wave; and (b) packet wave.

2.2. Coupled Normal Mode Theory

The expression of sound pressure under normal mode theory is [25]:

$$p(r, z) = \sum_{m=1}^M A_m(r) \psi_m(r, z), \quad (4)$$

where M is the number of modes, $A_m(r)$ is the amplitude of the m -th order local mode, and $\psi_m(r, z)$ is the characteristic function of the m -th order local mode.

In a range-dependent environment, the modal functions and eigenvalues exhibit dependence in the horizontal direction, and the coupled normal waves divide the horizontal direction r into several small intervals. The modal function $\psi_m^j(z)$ and the eigenvalue k_{rm}^j within the j -th interval can be obtained by solving the local characteristic equation:

$$\rho \left[\frac{\partial}{\partial z} \left(\frac{1}{\rho} \frac{\partial \psi_m^j(z)}{\partial z} \right) \right] + \left[\frac{\omega^2}{(c^j)^2} - (k_{rm}^j)^2 \right] \psi_m^j(z) = 0, \tag{5}$$

where ρ and c^j represent the density and the local sound speed. Calculate the amplitudes of different modes in each interval from near to far according to the horizontal distance. Taking the m -th mode at the horizontal distance r in the j -th interval as an example, the sound pressure can be described as [5]:

$$p_m^j(r, z) = \left[a_m^j \hat{H}_{(0),m}^{(1),j}(r) + b_m^j \hat{H}_{(0),m}^{(2),j}(r) \right] \psi_m^j(z), \tag{6}$$

where a_m^j and b_m^j are the modal coefficients for the j -th interval. $\hat{H}_{(0),m}^{(1),j}(r)$ is the zeroth-order first-kind Hankel function, which represents the forward-propagating acoustic field and $\hat{H}_{(0),m}^{(2),j}(r)$ represents the backward-propagating acoustic field. To effectively enhance computational efficiency with a minimal loss of accuracy, backward scattering is neglected, resulting in $\hat{H}_{(0),m}^{(2),j}(r)$ being ignored.

$$\hat{H}_{(0),m}^{(1),j}(r) = \frac{H_{(0)}^{(1)}(k_{rm}^j r)}{H_{(0)}^{(1)}(k_{rm}^j r_{j-1})}, \tag{7}$$

$$a^{j+1} = R_1^j a^j, \tag{8}$$

where a^{j+1} and a^j are the modal coefficient column vectors in the $j + 1$ -th interval and j -th interval. R_1^j is the transmission matrix:

$$R_1^j = \frac{1}{2} \left(C^{(1),j} + C^{(2),j} \right) H_{(0)}^{(1)}$$

where R_1^j and $(C^{(1),j} + C^{(2),j})$ are the $M \times M$ propagation and coupling matrices, and the elements of the coupling matrices are coupling coefficients:

$$c_{m,n}^j = \frac{1}{2} \left(1 + \frac{k_{rn}^j}{k_{rm}^{j+1}} \right) \int_0^\infty \frac{\psi_m^{j+1}(z) \psi_n^j(z)}{\rho(z)} dz, \tag{9}$$

Based on Equations (4)–(9), the TL can be described as [25]:

$$TL = 20 \log_{10} [p(r, z)], \tag{10}$$

The intensity of the m -th order mode can be described by the amplitude of each A_m mode [26]

$$I_m(r) = 10 \log_{10} [A_m(r) A_m^*(r)], \tag{11}$$

where $*$ is the conjugate transpose. The intensity of the m -th order mode to the n -th order mode is calculated as follows:

$$I_{m-n}(r) = 10 \log_{10} \sum_{i=m}^n [A_i(r) A_i^*(r)]. \tag{12}$$

3. Results

3.1. Impact of the Sound Source

To assess the influence of varying source conditions on TL, examining both the frequency of the source and the depth of the source, owing to the large number of acoustic field calculations involved, only a few representative examples are presented here as follows: the source frequencies are 200 Hz (low frequency) and 600 Hz (high frequency), and the two source depths are 10 m (mixed layer) and 50 m (lower mixed layer), resulting in a total of four combinations, as shown in Table 1.

Table 1. Classification of the sources.

Classification	Source Depth	Source Frequency
Situation 1	10 m	200 Hz
Situation 2	10 m	600 Hz
Situation 3	50 m	200 Hz
Situation 4	50 m	600 Hz

Figure 2 shows the TL plotted under the source conditions of situations 1–4, as shown in Table 1. The source is located at $R_s = 0$ m, and the receiver is located at $R_r = 33$ km and at depth $D_r = 40$ m (lower mixed layer). A LADS set at range $R_i = 2.4$ km is shown in Figure 1a ($R_i = 4$ km). The results show that the TL decreases as the depth of the source increases with the same source frequency: the TLs at 200 Hz and 600 Hz decrease by 7.5 dB and 8.3 dB, respectively, when the source depth shifts from the upper mixed layer to the lower mixed layer. This is because the source mainly excites the higher-order modes when the source is located in the upper mixed layer, and the loss of the higher-order modes in the process of propagation is faster. In contrast, the source mainly excites the lower-order modes when it is located in the lower mixed layer; thus, the loss of the lower-order modes is slower, and they are less affected by the thermocline or the ISW.

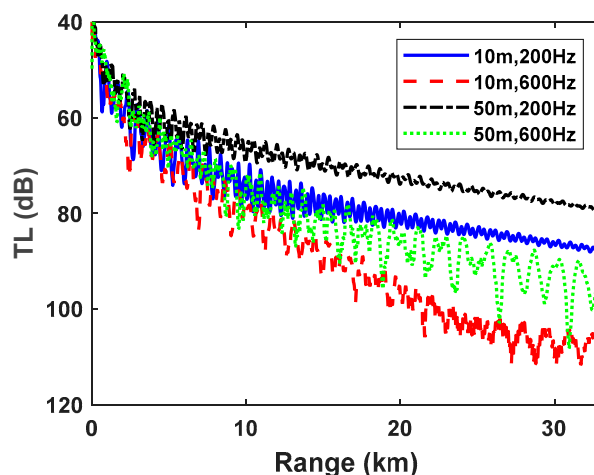


Figure 2. Comparison of different source conditions on the TL when $D_r = 40$ m. The blue line represents a source depth of 10 m and a source frequency of 600 Hz, the red line represents a source depth of 10 m and a source frequency of 200 Hz, the black line represents a source depth of 50 m and a source frequency of 200 Hz and the green line represents a source depth of 50 m and a source frequency of 600 Hz.

The TL decreases when the frequency of the source decreases at a given source depth. The TLs of the 10 m source and 50 m source increase by 12 dB and 13 dB, respectively, with an increasing frequency of the source. This is because, under low-frequency source

conditions, the number of excited normal modes is lower, and the coupling effect between normal modes is weaker. When the receiver at depth $D_r = 12$ m (upper mixed layer), we can obtain the same conclusion from the simulation experiment, although the difference in TL under different source conditions received at 12 m is not significant.

3.2. Impact of ISW Characteristics

To investigate the impact of an ISW's characteristics on the acoustic field, different ISW models are shown in Figure 1 at $R_i = 2.4$ km. In addition, the frequency of the source is set to 600 Hz, the source is set to a depth $D_s = 50$ m and the receiver is located at $R_r = 33$ km. The acoustic fields under the environments of the LADS, LADP, SADS and LAES are shown in Figure 3.

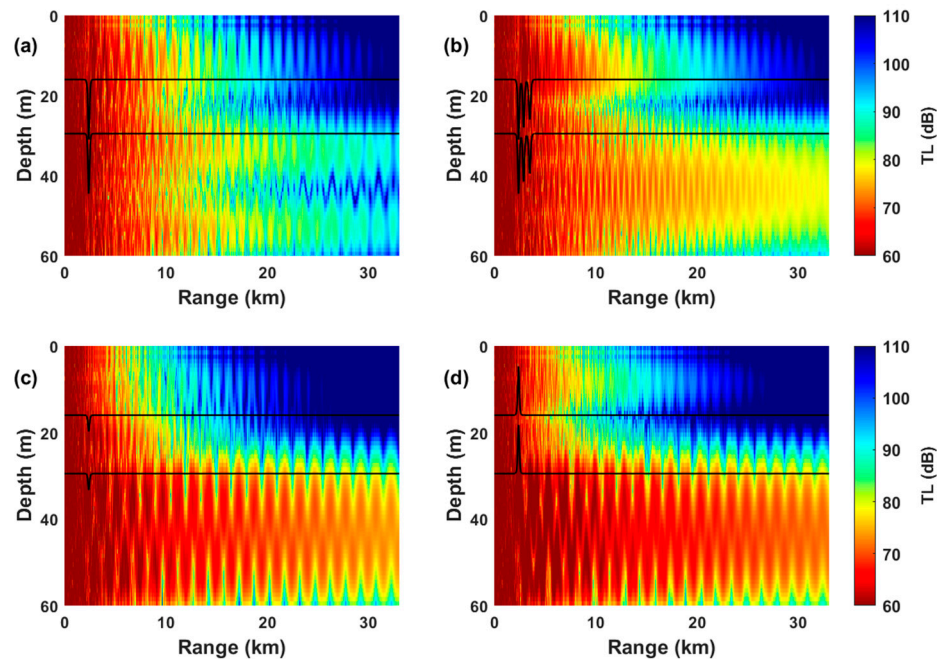


Figure 3. Comparisons of the acoustic fields with different ISWs; the thermocline displacement geometries are plotted as black lines. (a) LADS; (b) LADP; (c) SADS; and (d) LAES.

Figure 3 shows that the TL received at the lower mixed layer significantly increases in the LADS environment, as shown in Figure 3a. Figure 3b shows that the TL received at the upper mixed layer significantly decreases in the LADP environment. In addition, the TL received at the lower mixed layer attenuates very slowly in the SADS and LAES environments, as shown in Figure 3c,d. The results indicate that the different characteristics of the ISW mainly affect the upper mixed layer and lower mixed layer in the vertical direction and the middle and far distances of the sound field in the horizontal direction.

3.2.1. ISW Numbers

Figure 4 shows the TLs under the impact of the LADS, LADP and SADS, respectively, which correspond to Figure 3a–c. The blue line, red line and black line represent the soliton (large amplitude), packet and small amplitude, respectively.

When the receiver is in the upper mixed layer ($D_r = 12$ m), the difference in the TL between the LADS (blue line) and LADP (red line) environments changes relatively uniformly with distance, and the average reduction in the TL in the packet environment does not exceed 3 dB, as shown in Figure 4a. Comparing the LADS (blue line) and LADP (red line) environments, Figure 4b shows that the reduction in the TL received at the lower mixed layer ($D_r = 40$ m) in the packet environment increases with distance, with a maximum

decrease of approximately 25 dB. Therefore, under this source condition, an increase in the ISW number results in a decrease in the TL with a decreasing oscillation amplitude, especially when the depth of the receiver below the thermocline and the receiving distance are greater.

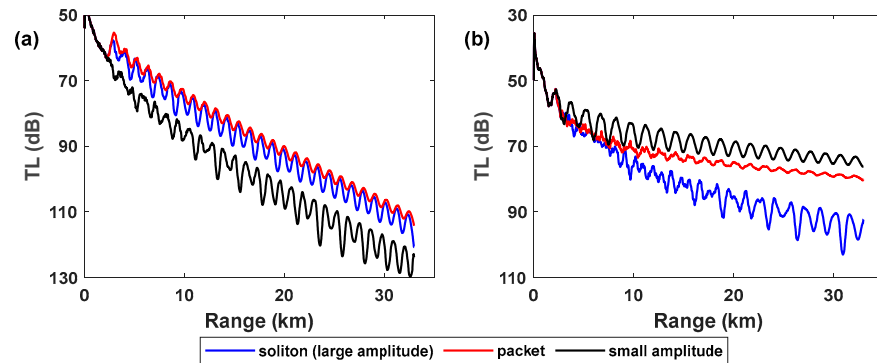


Figure 4. Comparison of the effects of different numbers and amplitudes of ISWs on the TL with distance variations when the source frequency is 600 Hz and $D_s = 50$ m: (a) Receiver at a depth of 12 m and (b) receiver at a depth of 40 m.

Figure 5a,b show TLs under the impact of the LADS and LADP with respect to the depth under different source conditions. The impact of the ISW number on the TL is primarily exerted at the lower mixed layer under different source conditions. Additionally, at the upper mixed layer, when the ISW number increases, the TL under all source conditions decreases by 1–2 dB, except for the shallow and high-frequency source conditions ($D_s = 10$ m, 600 Hz), for which the average increase in the TL is 6 dB. Figure 5b shows that when the ISW number increases, the shallow and high-frequency source conditions ($D_s = 10$ m, 600 Hz) represent the greatest reduction in the TL, with an average decrease of 13 dB; the deep and high-frequency source conditions ($D_s = 50$ m, 600 Hz) decrease by 11 dB at a depth of 43 m; the deep and low-frequency source conditions ($D_s = 50$ m, 200 Hz) are almost still; and the shallow and low-frequency source conditions ($D_s = 10$ m, 200 Hz) increase by 2 dB.

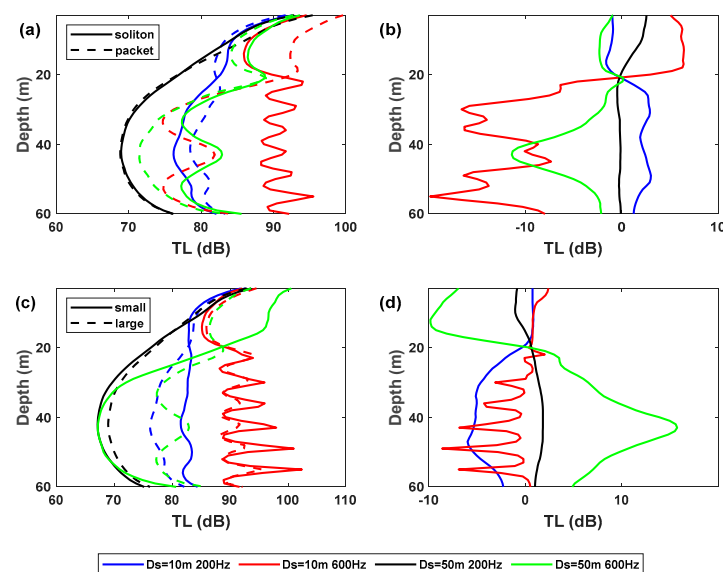


Figure 5. Comparison of the effects of different numbers and amplitudes of the ISW on the TL with depth variations: (a) TL between LADS and LADP; (b) difference in TL between LADS and LADP; (c) TL between LADS and SADS; and (d) difference in TL between LADS and SADS.

3.2.2. ISW Amplitudes

A comparison of TLs in the SADS (black line) and LADS (blue line) environments is shown in Figure 4. It reveals that when the amplitude of the ISW increases, an average decrease of 10 dB is received when the receiver is in the upper mixed layer ($D_r = 12$ m), and an average increase of 14 dB is received when the receiver is in the lower mixed layer ($D_r = 40$ m). Therefore, the increase in the amplitude of the ISW averages the acoustic energy distribution in the vertical direction of the receiver. Moreover, if the source is located in the upper mixed layer, the increase in the ISW amplitude will result in a decrease in the TL above the thermocline and an increase in the TL below the thermocline. Additionally, Figure 4a shows that at $D_r = 12$ m, the difference in the TLs under the SADS and LADS environments is uniform with increasing distance. Figure 4b shows that the difference in TLs under different ISW amplitude environments at the depth $D_r = 40$ m tends to increase with distance, up to a maximum of 30 dB.

Figure 5c,d show that when the amplitude of the ISW increases, the impact of the ISW amplitude on the TL is mainly exerted at the lower mixed layer under different source conditions. Additionally, at the upper mixed layer, when the ISW amplitude increases, the source conditions at deep and high frequencies ($D_s = 50$ m, 600 Hz) decrease significantly, with an average decrease of 8.6 dB in the TL. Figure 5d shows that when the ISW amplitude increases, the source conditions at shallow and low frequencies ($D_s = 10$ m, 200 Hz) have an average decrease of 5 dB in the TL; the source conditions at shallow and high frequencies ($D_s = 10$ m, 600 Hz) fluctuate more severely with an increasing depth, with an average decrease of 2 dB and a maximum reduction of 9 dB at a depth of 49 m; and the source conditions at deep and high frequencies ($D_s = 50$ m, 600 Hz) have a maximum increase of 16 dB at a depth of 43 m and a maximum reduction of 10 dB at a depth of 13 m.

3.2.3. ISW Polarity

To investigate the influence of the ISW polarity on the TL, the ISW environments of the LADS and LAES are considered. The TLs in each ISW environment are divided into several groups, of which the interval length is 10 dB, and the TL is assumed to be the interval centre of a certain group; then, the relative frequency $R(TL)$ is calculated with the following equation [27]:

$$R(TL) = \frac{N_i(TL)}{N}, \quad (13)$$

where $N_i(TL)$ is the number of samples in this group, and where N is the number of total samples. Figure 6 shows the relative frequency of the TL for the source in situations 1–4 when the polarity of the ISW changes.

In Figure 6, the TL received at the lower mixed layer (red bar; $D_r = 40$ m) is less than the TL received at the upper mixed layer (blue bar; $D_r = 12$ m). This phenomenon is clearly observed when the source depth is 50 m. Additionally, the range of the TL is wider when the frequency of the source is 600 Hz. This result shows that the impact of the source frequency on the TL is consistent with previous findings that showed that the TL increases when the source frequency increases. A comparison of Figure 6 reveals that the TL received at the lower mixed layer obviously changes when the ISW polarity changes from depressed (light-coloured bar) to elevated (dark-coloured bar). In the environment of an elevated ISW, when the TL is received at the lower mixed layer, the probabilities of the TL dominating within intervals of 95 dB, 105 dB, 65 dB and 65 dB, as shown in Figure 6, respectively. For example, in the lower mixed layer, the relative frequency of the TL within an interval of 65 dB in an elevated ISW environment is five times greater than that in a depressed ISW environment, as shown in Figure 6d. Therefore, the ISW polarity influences the TL received

at the lower mixed layer, especially when the source is located in the lower mixed layer where the elevated ISW decreases the TL.

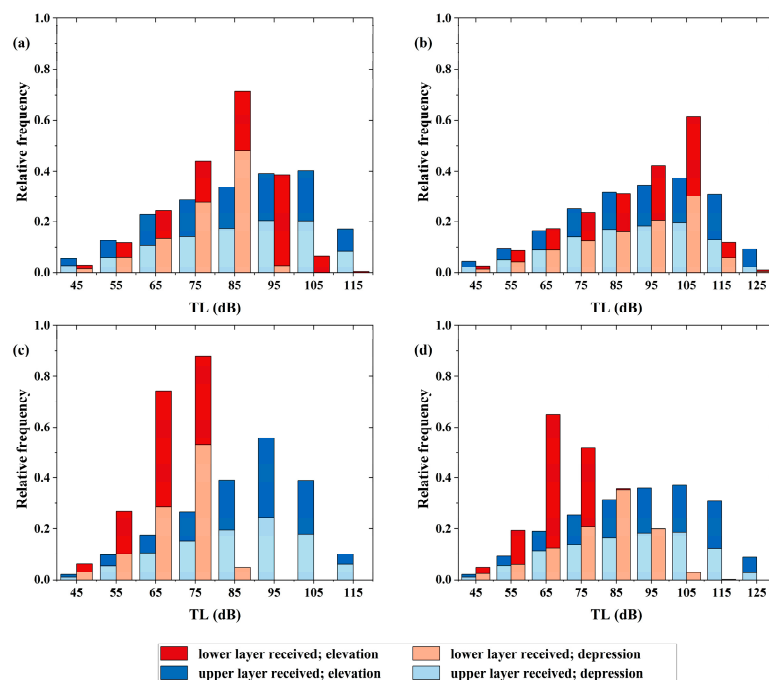


Figure 6. Comparison of the effects of different ISW polarities on the TL under different source conditions: (a) $D_s = 10$ m, 200 Hz; (b) $D_s = 10$ m, 600 Hz; (c) $D_s = 50$ m, 200 Hz; and (d) $D_s = 50$ m, 600 Hz.

Table 2 summarises the average TLs at depths of 15 m and 40 m and average depths in different ISW environments, i.e., LADS, LADP, SADS and LAES, corresponding to the acoustic field shown in Figure 3. The percentage in parentheses indicates the change in the TL relative to the TL under the ISW environment of the LADS, and a minus sign indicates a decrease in the TL. The results show that the TL received at a depth of 12 m is most affected by the ISW amplitude, and the TL increases by approximately 11% as the ISW amplitude decreases. At a depth of 40 m, the TL decreases by approximately 20% as the ISW polarity changes from the LADS to the LAES, and the ISW polarity also has the greatest impact on the TL at the average depth, with the TL decreasing by approximately 6%. Moreover, when both the ISW amplitude and the ISW polarity change, the TL received at 12 m increases; however, for the TL received at 40 m, the average depth decreases. Therefore, the TL received at all depths is affected primarily by the TL received at the lower mixed layer, considering the ISW amplitude and ISW polarity. In addition, the TL at a depth of average depth in the LADP environment is 83.7 dB, which is consistent with previous studies [10].

Table 2. Comparison of TLs with different ISWs when the source frequency is 600 Hz and $D_s = 50$ m.

	LADS	LADP	SADS	LAES
12 m	86.8 dB	84.5 dB (−2.65%)	96.6 dB (11.29%)	94.4 dB (8.76%)
40 m	81.3 dB	71.6 dB (−11.93%)	67.4 dB (−17.10%)	65.4 dB (−19.56%)
Depth average	87.1 dB	83.7 dB (−3.90%)	83.8 dB (−3.79%)	82.2 dB (−5.63%)

3.3. Impact of Moving ISW

To investigate the influence of the ISW position on the TL, a comparative analysis of the conclusions drawn from the SWARM experiment was conducted, with a source depth

of $D_s = 10$ m and a source frequency of 400 Hz. The position of the ISW was varied in increments of 100 m from the position of the source $R_s = 0$ km to the position of the receiver array $R_r = 33$ km. Figure 7 shows the TL at the receiving array $R_r = 33$ km under four different ISW environments, SADS, LADS, SAES and LAES, considering the impacts of the ISW amplitude and ISW polarity.

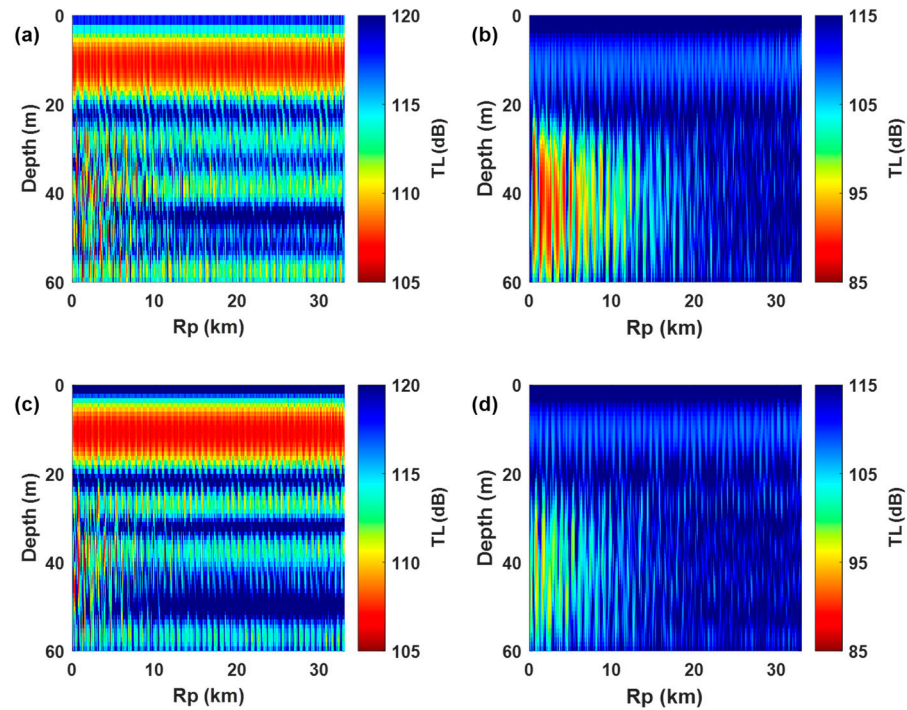


Figure 7. Relationship between the TL at the receiving array and the position of the ISW: (a) SADS; (b) LADS; (c) SAES; and (d) LAES.

Figure 7 shows that the variations in the ISW amplitude primarily affect the TL with depth. In an environment with a small-amplitude ISW, the energy is concentrated mainly in the upper mixed layer, whereas in an environment with a large-amplitude ISW, the energy propagates mainly towards the lower mixed layer. This result is consistent with the aforementioned conclusion that the increase in the amplitude of the ISW averages the acoustic energy distribution in the vertical direction. A comparison of Figure 7a,c reveals that when the polarity of the ISW changes from a depressed one to an elevated one, the energy transfers from the lower mixed layer to the upper mixed layer, resulting in a decrease of approximately 1 dB in the upper mixed layer and an increase of approximately 2 dB in the lower mixed layer. Comparing Figure 7b,d, the energy decreases by approximately 2 dB throughout the entire depth range when the polarity of the ISW changes from depressed to elevated.

Moreover, when both the ISW amplitude and the ISW polarity change, i.e., the amplitude of the ISW increases, the polarity of the ISW changes from depressed to elevated, and the TL decreases in the layer where the source is located. Therefore, compared with the change in the amplitude of the ISW, the change in the polarity of the ISW has a greater effect on the TL of the sound field at the receiver range of $R_r = 33$ km when the ISW moved from $R_p = 0$ km to $R_p = 33$ km. Additionally, as shown in Figure 7, as the position of the ISW approaches the source, the fluctuation in the sound energy at the average depth increases [10], and the fluctuation in the sound energy is significant in the lower mixed layer.

4. Discussion

To explain the numerical simulation experimental phenomena described in Section 3 and explore the mechanisms for the influence of changes in ISW characteristics on the TL, this section discusses the fluctuations in the intensity of the mode in different ISW environments.

The intensities of normal modes 1–6 in different ISW environments under the source of situation 4 ($D_s = 50$ m, 600 Hz) based on Equation (11) are shown in Figure 8. When the characteristics of the ISW change, the intensity of each normal mode varies significantly around the ISW [11]. Furthermore, since the source is below the thermocline and primarily excites the energy of lower normal modes, the dominant modes in terms of energy before being affected by the ISW are mode 1 and mode 2.

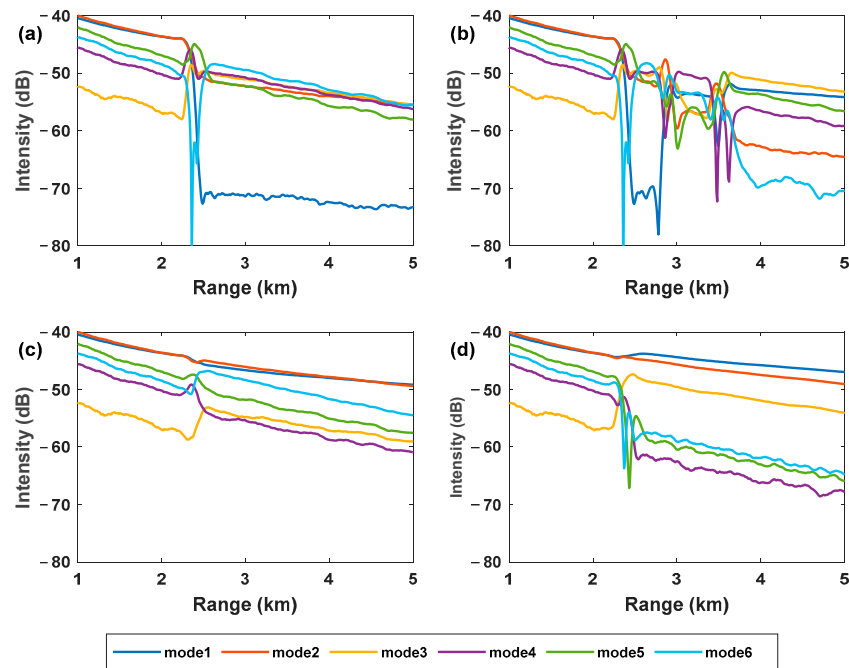


Figure 8. Intensity of modes 1–6 in different ISW environments: (a) LADS; (b) LADP; (c) SADS; and (d) LAES.

As shown in Figure 8a, in the LADS environment, the intensity of mode 1 experiences a significant loss, with a maximum fluctuation of approximately 28 dB; the energy of mode 1 mainly transfers to mode 6, which experiences an increase in sound intensity by approximately 2 dB. The energy is transferred mainly from lower-order modes to higher-order modes. Figure 8b shows normal modes in the LADP environment, where the coupling phenomenon between modes is enhanced. After encountering the ISW, the dominant modes in terms of energy are mode 1 and mode 3, and mode 6 has the greatest reduction. This indicates that under the impact of the packet, the energy of the higher-order modes transfers to the lower modes. Figure 8c shows that the fluctuation in intensity for each normal mode is relatively small in the small-amplitude ISW environment, which is consistent with the previous study [28]. The dominant mode almost remains, and the maximum fluctuations of the other coupled modes do not exceed 6 dB. In Figure 8d, after being affected by the elevated soliton, the dominant mode changes from mode 2 to mode 1, and the energy is coupled mainly between modes 3 and 6.

Considering the impact of the ISW on higher-order modes, the grouping of modes on the basis of Equation (12) is shown in Figure 9. Figure 9a shows the intensity of all the modes and presents the maximum fluctuation in the large-elevation soliton environment and the

minimum fluctuation in the LADS environment, which correspond to the influences of the ISW polarity and ISW amplitude variations on the TL, as previously mentioned. It can be observed that the intensity of modes 1–8 is almost equal to the total modal intensity, and modes 16–26 are almost unaffected by the variations in the ISW characteristics. Additionally, the intensity of modes 9–15 decreases slowly in the large-amplitude and depressed ISW environments, as shown in Figure 9c.

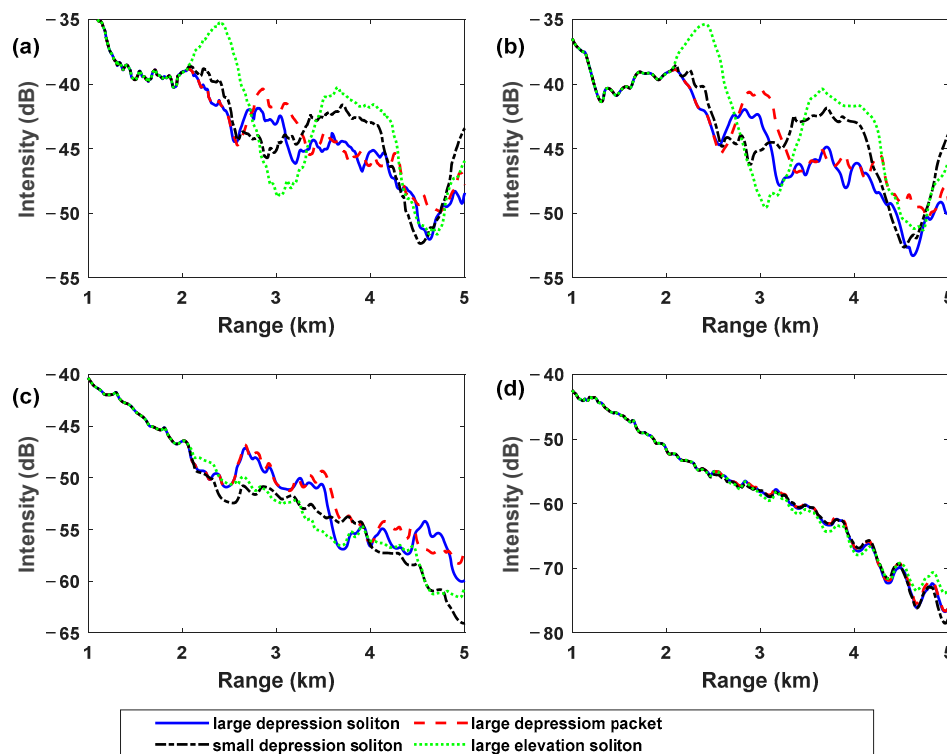


Figure 9. The sum of modal intensities in each group in different ISW environments: (a) Intensity of mode 1–26; (b) intensity of mode 1–8; (c) intensity of mode 9–15; and (d) intensity of mode 16–26.

In summary, the changes in intensity under the influence of the ISW sound field are due mainly to the mutual conversion of energy among different normal modes; when the characteristics of the ISW change, the energy coupling phenomenon between different normal modes is different. However, typically, when the energy transfers from higher-order to lower-order normal modes, the TL increases. Additionally, under this source condition, the intensity of modes 1–8 could represent all the intensities of all the modes, and the intensities fluctuate the most in large-elevation soliton environments.

5. Conclusions

In this study, simulation experiments were conducted by varying the source conditions and characteristics of an ISW. The variation in the sound energy received by the remote array influenced by the aforementioned factors is further discussed on the basis of coupled normal mode theory. The simulation results reveal that at the same source frequency, as the source depth increases, the TL decreases. At the same source depth, as the source frequency increases, the TL increases. As the ISW number increases, the TL decreases significantly below the thermocline when the source frequency is 600 Hz, with a maximum reduction of 20 dB. The increase in the amplitude of the ISW averages the acoustic energy distribution in the vertical direction of the receiver, with a more significant fluctuation in the TL below the thermocline in different source conditions. When the polarity of the ISW changes from depressed to elevated, the TL decreases when the source is in the lower mixed layer. Additionally, when the ISW moves from the position of the source at $R_p = 0$ km to the

position of the receiver at $R_p = 33$ km, the average sound energy fluctuation at the receiver weakens, and the impact of the changes in the polarity of the ISW on the TL is greater than that of the changes in the amplitude of the ISW.

The intensities of different modes individually and in groups under varying ISW environments were further explored, and it was found that when energy is transferred from lower-order to higher-order normal modes, the TL increases and vice versa. Moreover, under the source conditions of situation 4, the intensity of modes 1–8 could represent all the intensities of all the modes, and the intensities fluctuate the most in a high-elevation soliton environment.

This study is confined to the case of a translational ISW with a fixed geometry in a uniform waveguide. Other possible complex factors are not considered, including uneven seabed structures, undulating seabed topography, layered changes on a larger scale than the ISW and fronts near the ISW. All these factors can produce fluctuations, which may interfere with or mask the fluctuations caused by the mode coupling of the ISW. Further studies should explore the sound propagation characteristics when the complex factors mentioned above coexist with an ISW.

Author Contributions: Conceptualization, M.H.; Methodology, F.G.; Software, Y.Z. (Yongchui Zhang) and Y.W.; Writing—original draft, Z.L.; Writing—review & editing, Y.Z. (Yunxiang Zhang). All authors have read and agreed to the published version of the manuscript.

Funding: This research received no external funding.

Institutional Review Board Statement: Not applicable.

Informed Consent Statement: Not applicable.

Data Availability Statement: No new data were created or analyzed in this study. Data sharing is not applicable to this article.

Conflicts of Interest: The authors declare no conflict of interest.

References

1. Bourgault, D.; Galbraith, P.S.; Chavanne, C. Generation of internal solitary waves by frontally forced intrusions in geophysical flows. *Nat. Commun.* **2016**, *7*, 13606. [[CrossRef](#)]
2. Syamsudin, F.; Taniguchi, N.; Zhang, C.; Hanifa, A.D.; Li, G.; Chen, M.; Mutsuda, H.; Zhu, Z.N.; Zhu, X.H.; Nagai, T.; et al. Observing internal solitary waves in the Lombok Strait by coasta acoustic tomography. *Geophys. Res. Lett.* **2019**, *46*, 10475–10483. [[CrossRef](#)]
3. Jia, T.; Liang, J.; Li, X.M.; Sha, J. SAR observation and numerical simulation of internal solitary wave refraction and reconnection behind the Dongsha Atoll. *J. Geophys. Res. Oceans* **2018**, *123*, 74–89. [[CrossRef](#)]
4. Huthnance, J.M. Internal tides and waves near the continental shelf edge. *Geophys. Astrophys. Fluid Dyn.* **1989**, *48*, 81–106. [[CrossRef](#)]
5. Rouseff, D.; Turgut, A.; Wolf, S.N.; Finette, S.; Orr, M.H.; Pasewark, B.H.; Apel, J.R.; Badiéy, M.; Chiu, C.S.; Headrick, R.H.; et al. Coherence of acoustic modes propagating through shallow water internal waves. *J. Acoust. Soc. Am.* **2002**, *111*, 1655–1666. [[CrossRef](#)] [[PubMed](#)]
6. Headrick, R.H.; Lynch, J.F.; Kemp, J.N.; Newhall, A.E.; von der Heydt, K.; Apel, J.R.; Badiéy, M.; Chiu, C.S.; Finette, S.; Orr, M.H.; et al. Acoustic normal mode fluctuation statistics in the 1995 SWARM internal wave scattering experiment. *J. Acoust. Soc. Am.* **2000**, *107*, 201–220. [[CrossRef](#)] [[PubMed](#)]
7. Zhou, J.X.; Zhang, X.Z.; Rogers, P.H. Resonant interaction of sound wave with internal solitons in the coastal zone. *J. Acoust. Soc. Am.* **1991**, *90*, 2042–2054. [[CrossRef](#)]
8. Badiéy, M.; Katsnelson, B.G.; Lynch, J.F.; Pereselkov, S. Frequency dependence and intensity fluctuations due to shallow water internal waves. *J. Acoust. Soc. Am.* **2007**, *122*, 747–760. [[CrossRef](#)]
9. Duda, T.F. Acoustic mode coupling by nonlinear internal wave packets in a shelfbreak front area. *IEEE Ocean. Eng.* **2004**, *29*, 118–125. [[CrossRef](#)]
10. Duda, T.F.; Preisig, J.C. A modeling study of acoustic propagation through moving shallow-water solitary wave packets. *IEEE Ocean. Eng.* **1999**, *24*, 16–32. [[CrossRef](#)]

11. Preisig, J.C.; Duda, T.F. Coupled acoustic mode propagation through continental-shelf internal solitary waves. *IEEE Ocean. Eng.* **1997**, *22*, 256–269. [[CrossRef](#)]
12. Headrick, R.H.; Lynch, J.F.; Kemp, J.N.; Newhall, A.E.; von der Heydt, K.; Apel, J.; Badiy, M.; Chiu, C.S.; Finette, S.; Orr, M.H.; et al. Modeling mode arrivals in the 1995 SWARM experiment acoustic transmissions. *J. Acoust. Soc. Am.* **2000**, *107*, 221–236. [[CrossRef](#)]
13. Gao, F.; Hu, P.; Xu, F.; Li, Z.; Qin, J. Effects of Internal Waves on Acoustic Temporal Coherence in the South China Sea. *J. Mar. Sci. Eng.* **2023**, *11*, 374. [[CrossRef](#)]
14. Katsnelson, B.G.; Grigorev, V.; Badiy, M.; Lynch, J.F. Temporal sound field fluctuations in the presence of internal solitary waves in shallow water. *J. Acoust. Soc. Am.* **2009**, *126*, EL41–EL48. [[CrossRef](#)]
15. Badiy, M.; Katsnelson, B.G.; Lynch, J.F.; Pereselkov, S.; Siegmann, W.L. Measurement and modeling of three-dimensional sound intensity variations due to shallow-water internal waves. *J. Acoust. Soc. Am.* **2005**, *117*, 613–625. [[CrossRef](#)] [[PubMed](#)]
16. Luo, J.; Badiy, M.; Karjadi, E.; Katsnelson, B.; Tskhoidze, A.; Lynch, J.; Moum, J.N. Observation of sound focusing and defocusing due to propagating nonlinear internal waves. *J. Acoust. Soc. Am.* **2008**, *124*, EL66–EL72. [[CrossRef](#)] [[PubMed](#)]
17. Lynch, J.F.; Lin, Y.-T.; Duda, T.F.; Newhall, A.E. Acoustic ducting, reflection, refraction, and dispersion by curved nonlinear internal waves in shallow water. *IEEE Ocean. Eng.* **2010**, *35*, 12–27. [[CrossRef](#)]
18. Lin, Y.-T.; Duda, T.F.; Lynch, J.F. Acoustic mode radiation from the termination of a truncated nonlinear internal gravity wave duct in a shallow ocean area. *J. Acoust. Soc. Am.* **2009**, *126*, 1752–1765. [[CrossRef](#)] [[PubMed](#)]
19. Apel, J.R.; Ostrovsky, L.A.; Stepanyants, Y.A.; Lynch, J.F. Internal solitons in the ocean and their effect on underwater sound. *J. Acoust. Soc. Am.* **2007**, *121*, 695–722. [[CrossRef](#)] [[PubMed](#)]
20. Dozier, L.; Tappert, F. Statistics of normal mode amplitudes in a random ocean. I. Theory. *J. Acoust. Soc. Am.* **1978**, *63*, 353–365. [[CrossRef](#)]
21. Dozier, L.; Tappert, F. Statistics of normal mode amplitudes in a random ocean. II. Computations. *J. Acoust. Soc. Am.* **1978**, *64*, 533–547. [[CrossRef](#)]
22. Yang, T.C. Acoustic mode coupling induced by nonlinear internal waves: Evaluation of the mode coupling matrices and applications. *J. Acoust. Soc. Am.* **2014**, *135*, 610–625. [[CrossRef](#)]
23. Craig, W.; Guyenne, P.; Sulem, C. The surface signature of internal waves. *J. Fluid Mech.* **2012**, *710*, 277–303. [[CrossRef](#)]
24. Jiang, Y.; Grigorev, V.A.; Katsnel'son, B.G. Sound Field Fluctuations in Shallow Water in the Presence of Moving Nonlinear Internal Waves. *J. Mar. Sci. Eng.* **2022**, *10*, 119. [[CrossRef](#)]
25. Liu, J.; Piao, S.; Gong, L.; Zhang, M.; Guo, Y.; Zhang, S. The Effect of Mesoscale Eddy on the Characteristic of Sound Propagation. *J. Mar. Sci. Eng.* **2021**, *9*, 787. [[CrossRef](#)]
26. Gao, F.; Xu, F.; Li, Z.; Qin, J.; Zhang, Q. Acoustic propagation uncertainty in internal wave environments using an ocean-acoustic joint model. *Chin. Phys. B* **2023**, *32*, 034302. [[CrossRef](#)]
27. Liu, R.; Li, Z. Effects of rough surface on sound propagation in shallow water. *Chin. Phys. B* **2019**, *28*, 014302. [[CrossRef](#)]
28. Chiu, L.Y.S.; Reeder, D.B.; Chang, Y.-Y.; Chen, C.-F.; Chiu, C.-S.; Lynch, J.F. Enhanced acoustic mode coupling resulting from an internal solitary wave approaching the shelfbreak in the South China Sea. *J. Acoust. Soc. Am.* **2013**, *133*, 1306–1319. [[CrossRef](#)] [[PubMed](#)]

Disclaimer/Publisher's Note: The statements, opinions and data contained in all publications are solely those of the individual author(s) and contributor(s) and not of MDPI and/or the editor(s). MDPI and/or the editor(s) disclaim responsibility for any injury to people or property resulting from any ideas, methods, instructions or products referred to in the content.